



## Article

# Probabilistic Prediction and Assessment of Train-Induced Vibrations Based on Mixture Density Model

Ziyu Tao <sup>1,2</sup> , Lingshan He <sup>3</sup>, Desi Tu <sup>4</sup> and Chao Zou <sup>1,4,\*</sup> <sup>1</sup> State Key Laboratory of Performance Monitoring and Protecting of Rail Transit Infrastructure, East China Jiaotong University, Nanchang 330013, China; zi-yu.tao@polyu.edu.hk<sup>2</sup> The Aviation Services Research Centre, Hong Kong Polytechnic University, Hong Kong, China<sup>3</sup> Guangzhou Urban Planning and Design Survey Research Institute Co., Ltd., Guangzhou 510060, China<sup>4</sup> School of Civil and Transportation Engineering, Guangdong University of Technology, Guangzhou 510006, China

\* Correspondence: chao.zou@gdut.edu.cn

**Abstract:** This study presents a probabilistic prediction method for train-induced vibrations by combining a deep neural network (DNN) with the mixture density model in a cascade fashion, referred to as the DNN-RMDN model in this paper. A benchmark example is conducted to demonstrate and evaluate the prediction performance of the DNN-RMDN model. Subsequently, the model is applied to a case study to investigate and compare the uncertainties of train-induced vibrations in the throat area and testing line area of a metro depot. After training, the model is capable of accurately predicting the probability density function (PDF) of train-induced vibrations at different distances from the track and at different frequencies. Utilizing the predicted PDF, probabilistic assessments can be performed to ascertain the likelihood of surpassing predefined limits. By employing a mixture density model instead of a single Gaussian distribution, the DNN-RMDN model achieves more accurate prediction of the PDF for train-induced vibrations. The proposed probabilistic assessment framework can effectively assist in vibration screening during the planning phase and in selecting and designing vibration mitigation measures of appropriate levels.



**Citation:** Tao, Z.; He, L.; Tu, D.; Zou, C. Probabilistic Prediction and Assessment of Train-Induced Vibrations Based on Mixture Density Model. *Buildings* **2024**, *14*, 3468. <https://doi.org/10.3390/buildings14113468>

Academic Editor: Shaohong Cheng

Received: 9 October 2024

Revised: 26 October 2024

Accepted: 28 October 2024

Published: 30 October 2024



**Copyright:** © 2024 by the authors. Licensee MDPI, Basel, Switzerland. This article is an open access article distributed under the terms and conditions of the Creative Commons Attribution (CC BY) license (<https://creativecommons.org/licenses/by/4.0/>).

**Keywords:** metro depot; train-induced ground vibration; vibration variations; deep learning; residual mixture density network; probabilistic prediction and assessment

## 1. Introduction

Train-induced vibration has been a topic of concern in research for several decades. Excessive vibrations have the potential to cause discomfort to residents, malfunctions in vibration-sensitive equipment, and even damage to cultural heritage structures located in close proximity to the rail lines. In recent years, there has been an increasing emphasis on assessing the impact of train-induced vibrations on the serviceability of nearby buildings. This focus has been partly driven by the growing prevalence of transit-oriented development (TOD) in mega cities. The efficient prediction and evaluation of train-induced vibrations can support transit-oriented development (TOD) planning and aid in the decision-making process regarding the adoption of vibration control measures.

Train-induced vibration is essentially a random vibration phenomenon. However, most existing prediction methods [1–5] and evaluation standards [6,7] primarily focus on the deterministic behavior of train-induced vibrations, often overlooking their inherent randomness. It is widely recognized that vibration levels are influenced by the characteristics of vibration sources, propagation paths, and the recipients. In the case of train-induced ground-borne vibrations, the dynamics of trains, tracks, and the ground medium play a crucial role. Deterministic methods focus on predicting vibrations from the same train operating on the same track and neglect the uncertainty of vibration propagation caused by spatially varying soil properties. Therefore, for a given vibration source condition, such

as the train type, track structures, and operating speed, deterministic methods predict a constant vibration level at a specific location, assuming a simplified soil model, such as the frequently used layered soil model. The predicted constant vibration level generally represents the conditional average of field measurements incorporating uncertainties arising from both vibration source and propagation.

In practice, train-induced ground-borne vibrations often exhibit pronounced variations [8,9]. Consequently, even if the predicted conditional average of train-induced vibrations falls within the limits required by assessment standards, there is still a probability, to some extent, of causing disturbance to the environment. In this context, probabilistic prediction and assessment take precedence over their deterministic counterparts, as they provide a range within which train-induced vibrations are likely to occur. Moreover, probabilistic approaches assist in determining the optimal level of vibration control measures to be implemented.

The variations in field measurements of train-induced ground-borne vibrations stem from factors such as rail unevenness [10], wheel out-of-roundness [11], and the propagation uncertainty caused by spatially varied soil properties [12,13]. Currently, research on the random characteristics of the aforementioned factors primarily focuses on high-speed rail lines or subway mainlines, assuming a constant distance between the track and a fixed receiver location, as well as a consistent track structure. The metro depot is an auxiliary facility of the subway system where metro trains are parked, tested, maintained, and cleaned. Constructing over-track buildings above the metro depot not only effectively utilizes urban land resources but also facilitates the commuting of citizens living or working in the over-track community. Compared to buildings located near the high-speed rail lines or subway mainlines, the over-track buildings of a metro depot are subjected to a more complex vibration field, even though the train operation speed is slower. The variation in train-induced ground-borne vibrations within a metro depot is significant and worthy of investigation due to the following factors:

- (1) The large area occupied by a metro depot leads to significant variations in soil properties.
- (2) The different functional regions within the metro depot, such as the throat area, testing line area, and parking/maintenance area, showcase distinct train-induced vibration characteristics due to variations in operation speed and track structures.
- (3) The concurrent operation of different trains on various rail lines adds extra spatiotemporal complexity to the vibration source.
- (4) The irregular distribution of foundations for the over-track platform and buildings results in a complex diffraction field of train-induced vibrations.

Considering the complexity mentioned, the utilization of a combination of the Monte Carlo method and previously introduced deterministic methods to analyze the train-induced uncertainty within a metro depot becomes highly challenging [14] and demands significant computational resources. With the decreasing cost of data acquisition and developments in neural network models [15], as well as computing hardware, data-driven methods are gradually gaining attention for both deterministic predictions [16–22] and probabilistic predictions [23].

This research aims to fill the current research gap by providing probabilistic predictions and assessments of train-induced ground-borne vibrations in the metro depot with the presence of over-track buildings. An efficient probabilistic prediction method based on the deep learning approach and the mixture density model is proposed, which is referred to as the DNN-RMDN model in this paper. In this research, the mixture density model is utilized instead of the Bayesian neural network because the former is adept at capturing intricate, multi-modal output distributions, whereas the latter primarily focuses on estimating uncertainty by modeling the posterior distribution over the network weights. Thus, the proposed method enables the prediction of the probability density function (PDF) of train-induced ground-borne vibrations as a function of distance to the track and frequency. This facilitates probabilistic assessment and assists in making decisions regarding the extent to which vibration control measures should be designed and implemented.

## 2. Probabilistic Prediction Method Based on Mixture Density Model

This section introduces a mixture density model-based approach, referred to as the DNN-RMDN model in this study, which offers an efficient method for probabilistic prediction and the assessment of train-induced vibrations.

### 2.1. Methodology

The structure of the DNN-RMDN model is depicted in Figure 1. It consists of two cascaded submodels: a deep neural network (DNN) and a mixture density network (MDN).

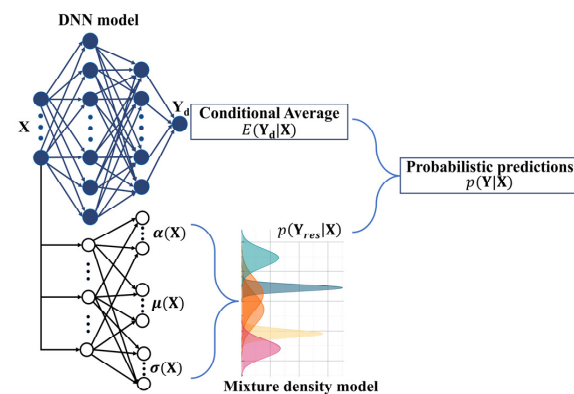


**Figure 1.** Structure of the DNN-RMDN model.

In the proposed DNN-RMDN model, a DNN is first employed to learn the relationship between the input factors  $\mathbf{X}$  and the conditional mean of random vibrations  $E(\mathbf{Y}_d | \mathbf{X})$ . For the application of the DNN model, min–max normalization is utilized on the datasets to aid in the optimization of the model. The rectified linear unit (ReLU) is used as the activation function within the DNN, enabling the introduction of non-linearity and enhancing the model's expressive power. The back-propagation technique, with the Adam algorithm, is utilized to train the DNN model. During training, the mean squared error serves as the loss function, guiding the optimization process.

Following the acquisition of predictions for the conditional average, the mixture density model [24] is employed to learn the probability distribution of the residuals  $p(\mathbf{Y}_{res} | \mathbf{X})$ . The  $p(\mathbf{Y}_{res} | \mathbf{X})$  is represented as a linear combination of Gaussian kernels, given by Equation (1) [24,25]:

$$p(\mathbf{Y}_{res} | \mathbf{X}) = \sum_{i=1}^k \alpha_i(\mathbf{X}) \cdot \frac{1}{\sqrt{2\pi}\sigma_i(\mathbf{X})} e^{-\frac{1}{2} \left( \frac{\mathbf{Y}_{res} - \mu_i(\mathbf{X})}{\sigma_i(\mathbf{X})} \right)^2} \quad (1)$$

where  $\alpha_i(\mathbf{X})$ ,  $\mu_i(\mathbf{X})$ , and  $\sigma_i(\mathbf{X})$  represent the mixing coefficient, mean, and standard deviation of the  $i$ th Gaussian kernel, respectively. Within the RMDN model, the logarithmic likelihood loss ( $-\log(p(\mathbf{Y}_{res} | \mathbf{X}))$ ) is employed as the loss function, while the tanh function serves as the activation function [26]. From the outputs of the RMDN model, the mean and standard deviation of input samples can be evaluated as follows [25]:

$$\mu(\mathbf{Y}_{res} | \mathbf{X}) = \sum_{i=1}^k \alpha_i(\mathbf{X}) \cdot \mu_i(\mathbf{X}) = 0 \quad (2)$$

$$\sigma(\mathbf{Y}_{res} | \mathbf{X}) = \sqrt{\sum_{i=1}^k \alpha_i(\mathbf{X}) \cdot (\sigma_i(\mathbf{X})^2 + \left\| \mu_i(\mathbf{X}) - \sum_{j \neq i} \alpha_j(\mathbf{X}) \cdot \mu_j(\mathbf{X}) \right\|^2)} \quad (3)$$

Because the conditional mean is extracted by the DNN model and the dataset residuals are then utilized for training the mixture density model, the mean calculated using Equation (2) equates to zero. This approach helps in simplifying the dataset complexity for the mixture density model through the detrending effect accomplished by the preceding DNN model. The RMDN model can be utilized to capture the inherent variability, known as aleatoric uncertainty, within the residual datasets. By adjusting the hyperparameters of the RMDN model, the epistemic uncertainty can be partially mitigated.

## 2.2. Benchmark Example

To verify the predictive accuracy of the proposed probabilistic method, a benchmark example is conducted in this section.

The dependent variable  $Y$  is composed of a deterministic component  $Y_d$  and a random component  $Y_r$ , as  $Y = Y_d + Y_r$ .

The deterministic component  $Y_d$  is the function of independent variables  $x_1$  and  $x_2$ , and is defined as follows:

$$Y_d(x_1, x_2) = 120 - (x_1 - 5)^2 - 5x_2 \quad (4)$$

The random component  $Y_r$  follows a normal distribution, where the mean is 0 and the standard deviation is a function of the independent variable  $x_1$ , i.e.,  $Y_r \sim N(0, \sigma^2(x_1))$ . The standard deviation function is defined as follows:

$$\sigma(x_1) = (x_1 + 1.8)/2 \quad (5)$$

In the benchmark example, eleven values of  $x_1$  (equally spaced values from 1 to 11) and three values of  $x_2$  (0, 6, 9) are used to determine the deterministic component  $Y_d$ , and a hundred samples for each  $x_1$  are generated to account for the variations in  $Y$ , i.e., the random component  $Y_r$ . Thus, a total of 3300 discrete data samples of  $Y$  are generated.

Using the method described in Section 2.1, a deep neural network (DNN) is first trained to predict the deterministic component  $Y_d$ . The adopted DNN model contains two inputs standing for values of independent variables  $x_1$  and  $x_2$ , respectively, and one output standing for the value of dependent variable  $Y$ . Figure 2a illustrates the predicted conditional mean from the trained DNN and the corresponding training datasets. Figure 2b shows the percentage error between the conditional mean predicted by the trained DNN and the corresponding training datasets. The percentage error is observed to be within 3%, indicating a high level of accuracy. This suggests that the DNN model has been effectively trained and can reliably predict the conditional average of  $Y$  for a given pair of input  $x_1$  and  $x_2$ .

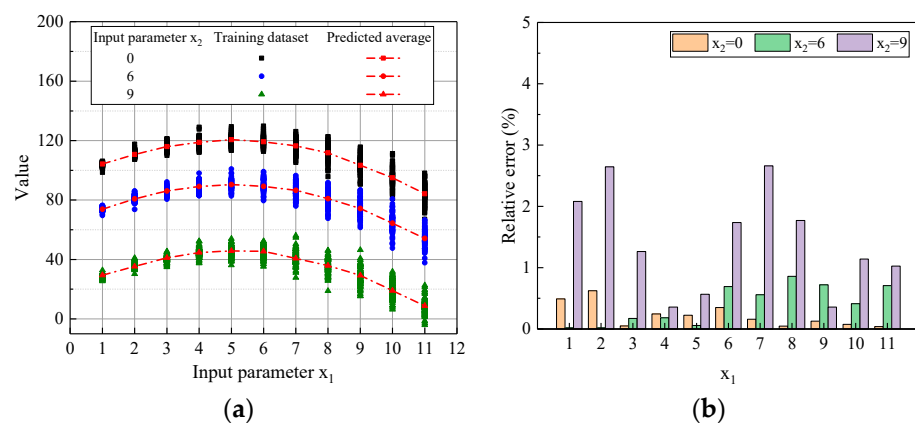


**Figure 2.** Training results of DNN for predicting the deterministic component. (a) Predicted mean and training datasets. (b) Percentage error of the trained DNN.

As described in Section 2.1, a followed residual mixture density network was trained to predict the random component  $Y_r$ . One hidden layer of 5 neurons and 2 Gaussian kernels was used to build the RMDN. Figure 3 displays the training result of the RMDN. The PDFs of two weighted Gaussian kernels as a function of  $x_1$  are shown, along with their linear combination at each value of  $x_1$ . It was observed that kernel 2 outweighs kernel 1, resulting in the linear combination predominantly following the weighted kernel 2. Furthermore, the PDF of an equivalent single Gaussian distribution, with its mean and standard deviation calculated from Equations (2) and (3), respectively, is superimposed on Figure 3.



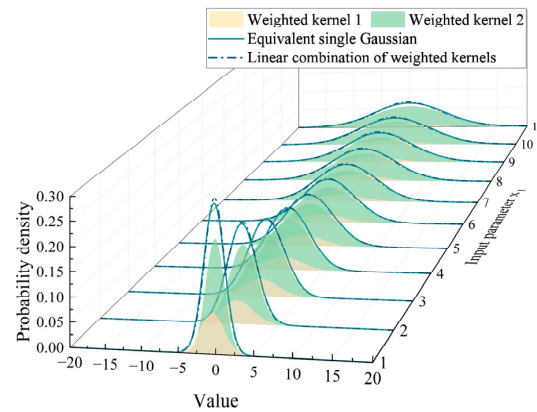


**Figure 3.** Training results of RMDN for predicting the random component.

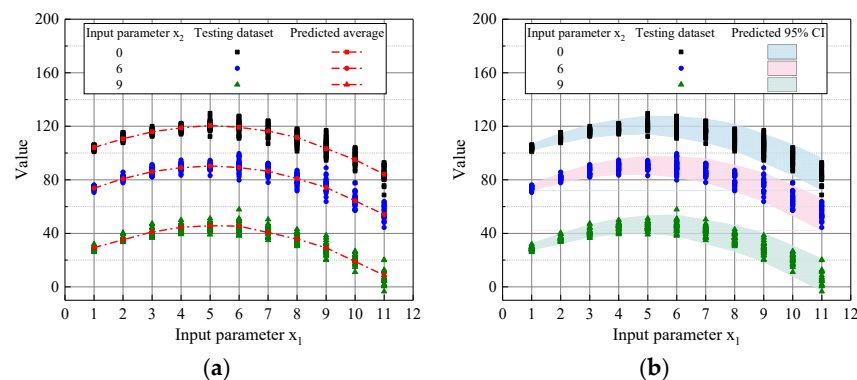
Since the samples of the random component in this benchmark example follow a normal distribution as shown in Equation (5), the difference between the actual PDF predicted by the linear combination of Gaussian kernels and the equivalent single Gaussian distribution is negligible. The results also indicate that the inclusion of additional Gaussian kernels in the RMDN will not compromise the model's prediction performance.

Table 1 compares the true standard deviations used in the benchmark example, calculated from Equation (5), with the corresponding predictions from the trained RMDN for each value of  $x_1$ . The results indicate that the RMDN is well-trained, with relative errors of standard deviation predictions within 5%.

**Table 1.** Identification accuracy of the standard deviation.

$x_1$	TRUE	Neuron5, $m = 2$	Relative Error (%)
1	1.4	1.4	1.4
2	1.9	2.0	5.8
3	2.4	2.5	5.4
4	2.9	3.0	4.5
5	3.4	3.6	4.7
6	3.9	4.1	4.9
7	4.4	4.6	5.0
8	4.9	5.1	4.1
9	5.4	5.5	2.4
10	5.9	5.9	0.2
11	6.4	6.2	3.4

Figure 4a,b shows the testing results for the deterministic component and random component, respectively. Like the training results, the trained DNN-RMDN well predicted the deterministic and random components of unseen testing data, which implies the proposed method can effectively quantify the inherent data randomness.



**Figure 4.** Testing results of the trained DNN-RMDN model. (a) Deterministic predictions. (b) Probabilistic predictions.

### 3. Application of the DNN-RMDN Model to Probabilistic Predict Train-Induced Vibrations

As discussed in the Introduction section, the vibration field induced by trains in a metro depot is intricate due to the complex configurations involving track locations and the presence of underground foundation structures, as depicted in Figure 5.

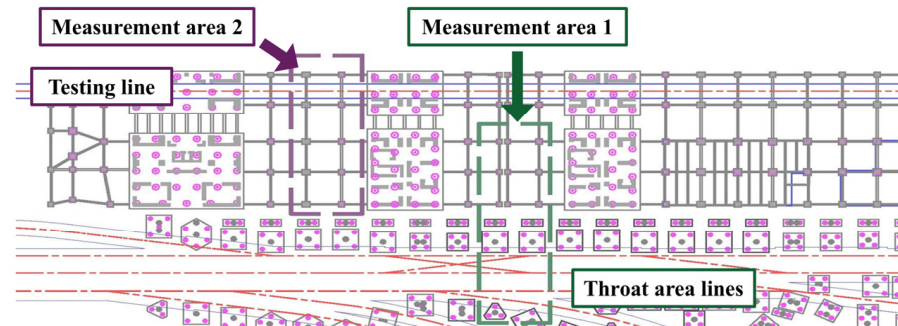


**Figure 5.** Layout of rail lines and underground foundations in a metro depot with over-track buildings.

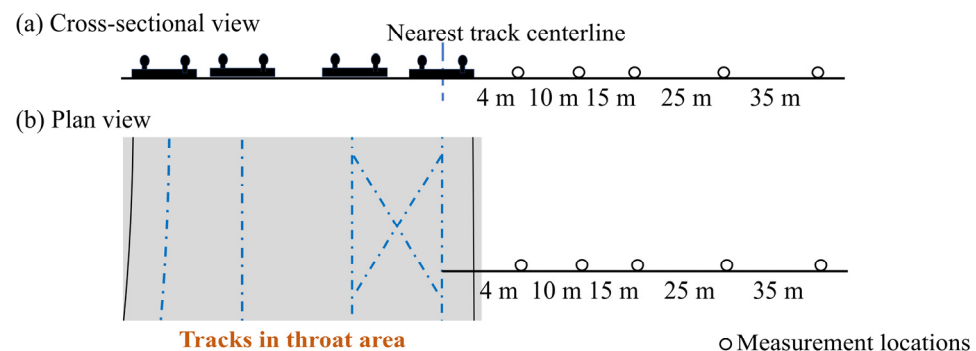
Two measurement campaigns were conducted to investigate and quantify the variations in train-induced ground-borne vibrations caused by train passages. These two campaigns specifically focused on the throat area and the testing line, respectively, whose measurement areas are shown in Figure 5. Both measurement campaigns utilized a sampling frequency of 1024 Hz, which is adequate for analyzing frequencies of interest up to 80 Hz. Additional information regarding the measurement equipment, the operating metro train, soil properties, and the track structures can be found in [4,5,9].

For the measurement campaign in the throat area, the ground-borne vibrations were recorded at multiple locations while the investigated metro trains passed through different rail lines in the throat area. For the measurement campaign in the testing area, the ground-borne vibrations were recorded at multiple locations while the same train operated back and forth on the testing line. The variation in train-induced vibrations in the throat area is greater than that in the testing line. This is attributed to the increased uncertainties arising from the vibration source, such as the variation in out-of-roundness among different trains, the uncertainty in the exact distance between the operated rail line in the throat area and the measured location, and the variability in train operation speeds.

#### 3.1. Vibration Variations in the Throat Area

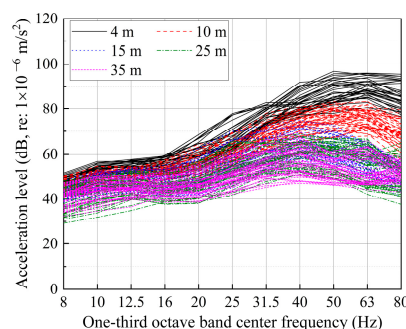
##### 3.1.1. Field Measurement Setups

Figure 6 illustrates a schematic diagram of the plan view and cross-sectional view of the measurement setups in the throat area. Five locations on the ground surface, positioned at distances of 4 m, 10 m, 15 m, 25 m, and 35 m from the center line of the nearest track in the throat area, were equipped with accelerometers to record train-induced vibrations during various train passages in the throat area.



**Figure 6.** Field measurement setups in the throat area.

Figure 7 shows the one-third octave band spectra of measured train passages at five locations with different distances to the throat area. The analysis was conducted within the frequency range of 8 to 80 Hz, which is of interest for the study [7]. The dominant frequencies were observed to be in the range of 40 to 80 Hz. As the distance from the throat area increases, the dominant frequencies tend to shift towards lower frequency bands. The separation of spectra between different locations becomes more pronounced at frequencies above 25 Hz, particularly for locations that are closer to the throat area. These phenomena can be attributed to the fact that higher frequency components decay more rapidly with distance compared to lower frequency components.



**Figure 7.** Measured vibration spectra of different train passages at various locations in the throat area.

When examining the vibration spectra at the same location, induced by different train passages in the throat area, it is observed that the acceleration level difference can reach up to 20 dB. Notably, this difference persists even when the vibrations are induced by trains of the same type, passing across the test section at a similar low speed range of 5 to 15 km/h. The variations in measurements at a fixed location are primarily attributed to several factors. Firstly, the wheel out-of-roundness configurations differ among different trains, contributing to measurement variations. Secondly, there is uncertainty regarding the exact distance between the operated rail line and the receiver location in the throat area, as the datasets do not differentiate which train passage operated on which rail line. Additionally, the uncertainty in vibration propagation arises from the spatially varied soil properties and the presence of irregular foundations of the over-track platform and buildings within the soil. These factors collectively contribute to the overall measurement variations observed.

### 3.1.2. Architecture Determination of the DNN-RMDN Model

This section is dedicated to establishing the architecture of the DNN-RMDN model, as shown in Figure 1. The DNN model is utilized to predict conditional means of vibration levels, while the RMDN model is employed to estimate the uncertainty linked to the predicted mean from the DNN model.

In this research, the DNN model utilizes two inputs: the distance between observation points and the track, and the one-third octave band center frequency. This choice is motivated by two reasons. Firstly, the datasets employed to build the DNN-RMDN model are collected from the same site, featuring the same type of metro trains and negligible variations in train speeds. Consequently, the vibration source and transmission path for the dataset are consistent. The primary factors influencing the vibration levels in the datasets are the distance and the evaluated center frequency, as demonstrated in Figure 7.

On the other hand, one practical application of the DNN-RMDN model is to facilitate the probabilistic assessment of train-induced vibrations, as illustrated in Section 4. When planning and designing railway constructions adjacent to existing buildings or constructing buildings near existing tracks, it is crucial to estimate the vibration levels and the probability of exceeding thresholds based on the distance and the evaluated frequency. These two factors are integral to evaluation standards and are of interest to stakeholders. Therefore, the inputs for the DNN model are chosen as the distance and the center frequency.

In addition, as seen in Figure 7, the variations in vibration levels are not clearly changed with the distance. Thus, the RMDN model's input is simplified to frequency only. Frequency-dependent uncertainty estimations for building serviceability assessments and vibration control measure designs and selection because they are frequency-specific. Furthermore, as depicted in Figure 7, the fluctuations in vibration levels do not exhibit significant changes with distance. Therefore, the input for the RMDN model is simplified to only include frequency. Frequency-dependent uncertainty estimations are crucial for building serviceability assessments and the design and selection of vibration control measures, as they are specific to different frequencies.

A total of 51 synchronized train passages were collected for each of the five locations, with an analysis of 11 center frequencies ranging from 8 to 80 Hz, resulting in a combined total of 2808 samples. Among them, 1966 randomly selected samples were allocated for the training dataset, with 842 samples designated for the testing dataset.

For the DNN model, pyramidal architecture was utilized with three hidden layers: 50 neurons in the first layer, 30 neurons in the second layer, and 20 neurons in the third layer, as detailed in the published work [21]. The learning rate employed was 0.001.

Figure 8a illustrates the mean squared error of the DNN model as the training epochs increase, showing convergence at 400 epochs. Figure 8b compares the predictions from the trained DNN model with the corresponding testing datasets. A linear regression with an  $R^2$  value of 0.850 indicates a strong correlation between them, suggesting that the trained DNN model performs effectively with the unseen testing datasets.

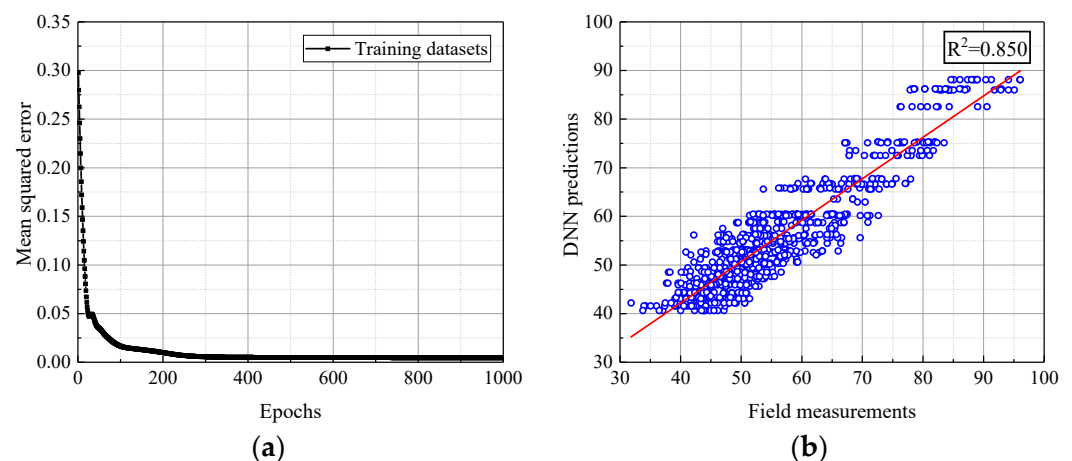


**Figure 8.** DNN model validation. (a) Training process; (b) testing results.

A shallow one-layer MLP was employed for the RMDN model since the conditional means were already extracted by the DNN model, and the distributions of residues were simplified through detrending. The hyperparameters of the RMDN model involve the number of neurons in the hidden layer of the MLP and the quantity of Gaussian kernels incorporated in the mixture density model.

The RMDN architecture was chosen based on the standard deviation computed from Equation (3). In Figure 9a, variations in calculated standard deviations at 31.5 Hz are depicted with different numbers of neurons in the hidden layer of the MLP and various numbers of Gaussian kernels within the mixture density model. Notably, the standard deviation of the dataset's residuals shows minimal sensitivity to the number of neurons in the 1-layer MLP, aligning with the detrending process where the means predicted by the DNN model are subtracted from the training dataset. Figure 9b illustrates the variations in calculated standard deviations as the number of Gaussian kernels increases. It is observed that with fewer than 20 Gaussian kernels, there is a decreasing pattern in the estimated standard deviation. This suggests that an order of the mixture density model exceeding 20 is necessary to effectively capture the randomness in the dataset's residuals. Thus, the chosen architecture for the RMDN model comprises a one-layer MLP with 10 neurons

and a mixture density model with 20 Gaussian kernels. Figure 9c displays the negative log-likelihood loss function of the RMDN model, converging at 2500 epochs. The learning rate utilized is 0.0001. The error analysis, validation process, and uncertainty quantification utilizing the outcomes of the DNN-RMDN model are discussed in the subsequent section.

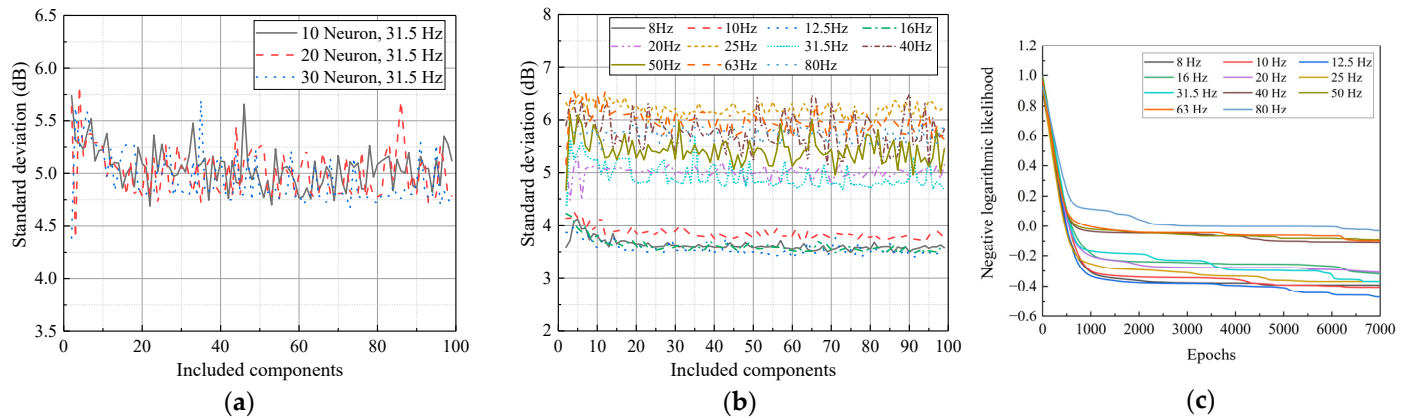


**Figure 9.** Sensitivity analysis for number of hidden neurons and Gaussian kernels: (a) effects of numbers of neurons and Gaussian kernels on  $\sigma$  at 31.5 Hz; (b) effects of numbers of Gaussian kernels on  $\sigma$  at different frequencies; (c) training process.

### 3.1.3. Quantifying Uncertainty with PDF

This section presents the training and testing outcomes of the DNN-RMDN model developed in Section 3.1.2. It showcases the predicted PDFs of train-induced vibrations in the throat area at each center frequency of the one-third octave band ranging from 8 to 80 Hz. These PDFs serve as a means to quantify the uncertainty associated with the vibrations.

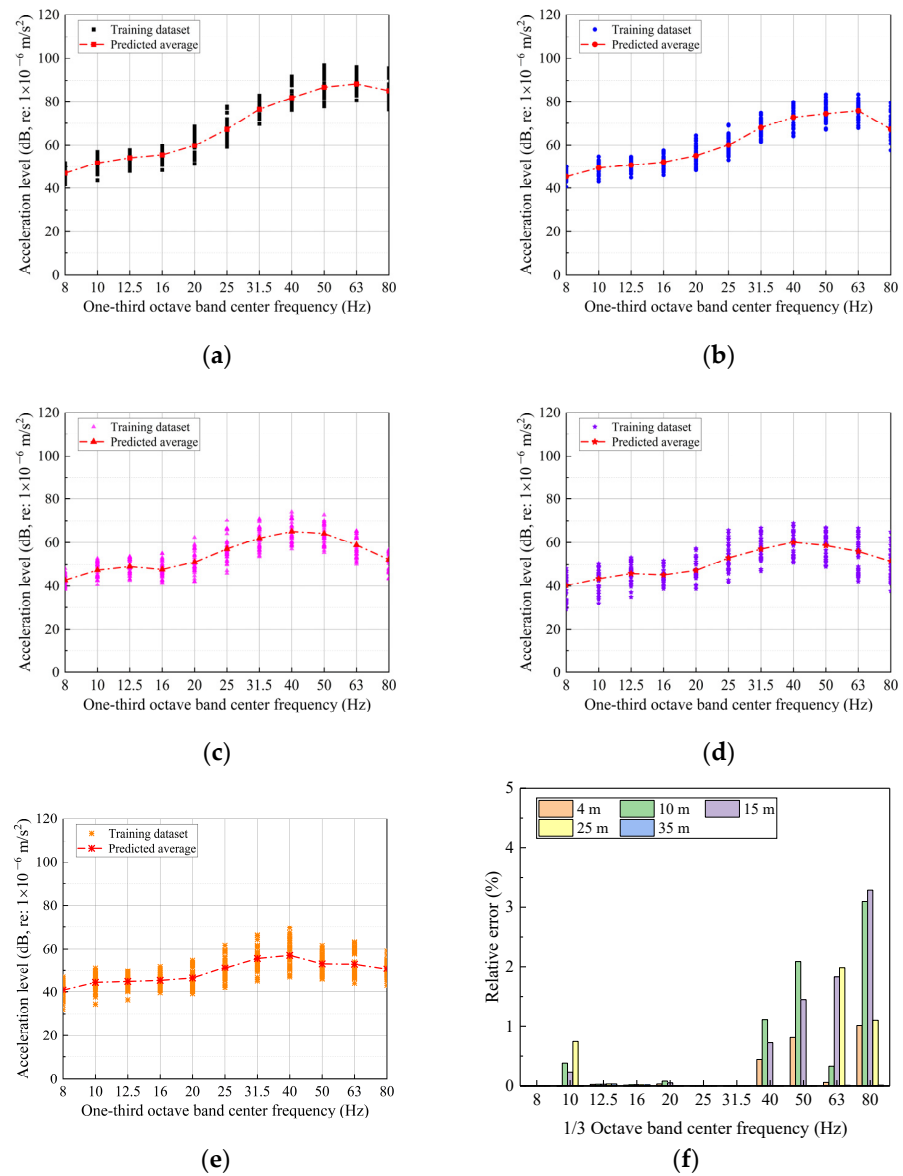
Figure 10 compares the predicted conditional averages of train-induced vibrations at the five measured locations using the trained DNN model to the training datasets. The percentage error is noted to be below 3.5%, as indicated in Figure 10f. It can be found that the DNN model is effectively trained and capable of accurately capturing the conditional average train-induced acceleration levels at each center frequency and measurement location.

After predicting the conditional averaged vibrations, the residuals of the datasets are calculated by subtracting the train-induced acceleration levels at each location from their corresponding conditional averages. The residual datasets represent the random component of train-induced vibrations and are then utilized for training the RMDN model to predict the PDF which has a zero mean.

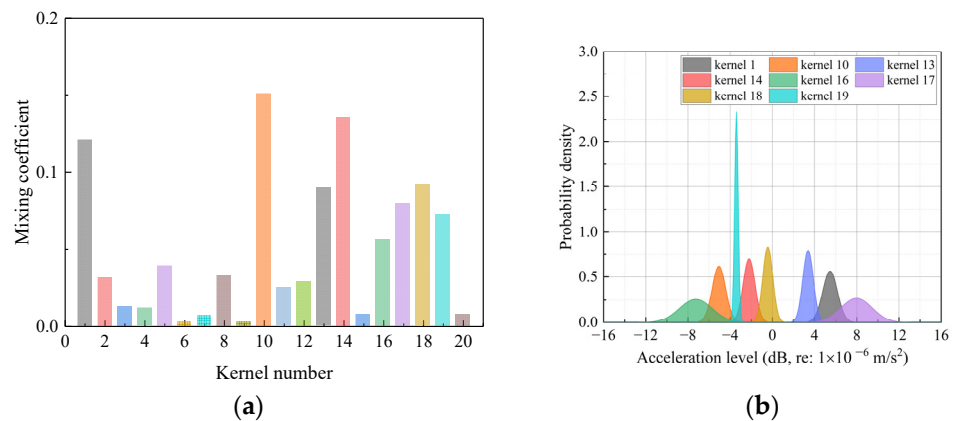
Figure 11a illustrates the mixing coefficients of the 20 Gaussian kernels in the mixture density model after training the DNN-RMDN model. Figure 11b displays the PDFs of the kernels with significant mixing coefficients. The PDFs of the kernels with large mixing coefficients are significant because they represent the distributions that contribute the most to the overall PDF estimation. These kernels capture the patterns and characteristics of the residual dataset that have a higher likelihood of occurring.

Figure 12 compares the overall PDF of residual train-induced vibrations at 31.5 Hz, based on the mixture density model consisting of a linear combination of 20 weighted Gaussian kernels as shown in Figure 11, to the equivalent single Gaussian distribution with a mean of zero and standard deviation calculated from the residual datasets using Equation (3). It is evident that the mixture density model has the capability to capture complex PDFs compared to a single Gaussian assumption. As a result, the PDF of train-induced vibrations predicted by the DNN-RMDN model offers greater accuracy in probabilistic assessment. This will be further explored and discussed in Section 4, where a comprehensive probabilistic assessment will be conducted.





**Figure 10.** Predictions of conditional averaged vibrations using a trained DNN model: (a) 4 m; (b) 10 m; (c) 15 m; (d) 25 m; (e) 35 m; (f) relative error.



**Figure 11.** Mixing coefficients and Gaussian kernels PDF with larger coefficient (31.5 Hz): (a) mixing coefficients; (b) kernels with large mixing coefficient.

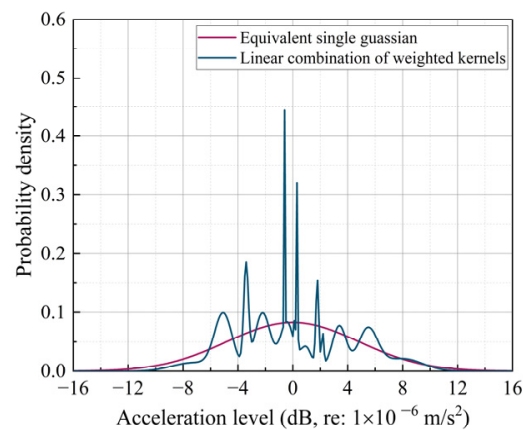


**Figure 12.** Comparisons of the PDF predicted with the RMDN model and the Gaussian distribution.

Figure 13 presents the predicted PDFs of residual train-induced vibrations by the RMDN model at various center frequencies. It is observed that the RMDN model's predicted PDFs exhibit different shapes at different center frequencies. This finding validates the assumption that the uncertainty of train-induced vibrations is indeed related to the frequency, as the PDF shapes vary accordingly.

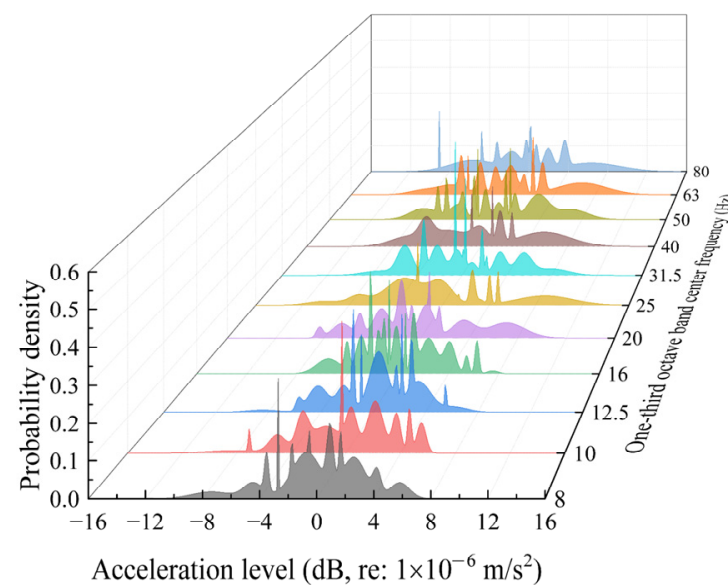


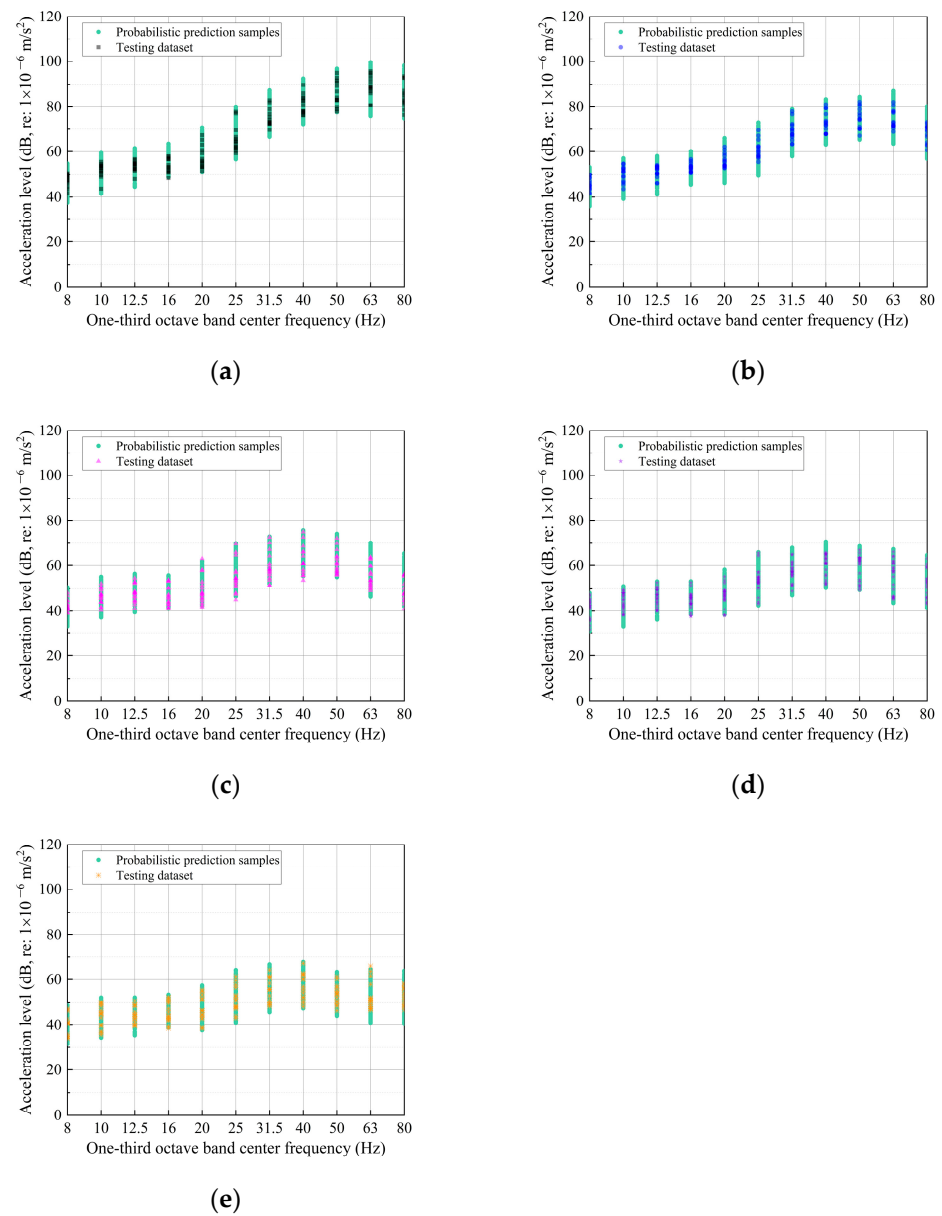
**Figure 13.** PDFs predicted with RMDN model at different center frequencies.

By utilizing the conditional average acceleration levels predicted by the DNN model at each measurement location, in combination with the RMDN model's predicted residual PDFs at each frequency, it is easy to obtain the PDFs of train-induced vibration levels at each measurement location and frequency. For each measurement location, 100 samples of acceleration-level spectra are generated. In Figure 14, these 100 samples are superimposed with the unseen testing dataset acquired from field measurements. The alignment between the testing dataset and the samples derived from the PDFs predicted by the trained DNN-RMDN model is evident. This validation provides confirmation of the proposed model's probabilistic prediction capability.

### 3.2. Vibration Variations in the Testing Line Area

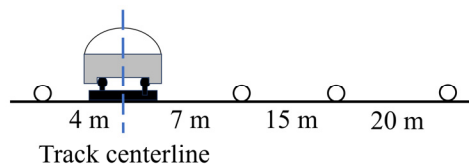
#### 3.2.1. Field Measurement Setups

Figure 15 illustrates a schematic diagram of the plan view and cross-sectional view of the measurement setups in the testing line area.

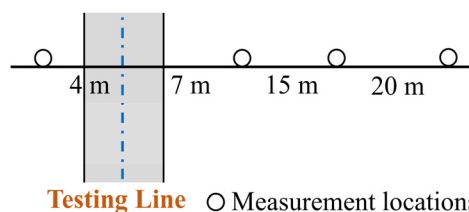


**Figure 14.** Performance test of the trained DNN-RMDN model: (a) 4 m; (b) 10 m; (c) 15 m; (d) 25 m; (e) 35 m.

(a) Cross-sectional view



(b) Plan view



Testing Line ○ Measurement locations

**Figure 15.** Field measurement setups in the testing line area.

Figure 16 shows the one-third octave band spectra of measured train passages at the four locations with different distances to the track center line of the testing line. The general trend in train-induced ground-borne vibrations in the testing line area mirrors that in the throat area. Specifically, higher-frequency vibration components exhibit a faster decay with distance, and the variation in vibrations is more closely related to frequency rather than the distance from the track. However, there are two distinct differences between train-induced ground-borne vibrations within the testing line area and the throat area. Firstly, when comparing Figure 16 to Figure 7, it is found that the frequency components between 63 Hz and 80 Hz are more prominent in ground-borne vibrations resulting from train passages on the testing line than those in the throat area. Secondly, it is noticeable that the variations in vibrations within the testing line area are significantly reduced compared to those in the throat area. This reduction can be attributed to the field campaign conducted on the testing line, where the same train operated on the same track, thereby minimizing the uncertainties induced by different trains of the same type and the distance between the operating rail line and the receiver location. Furthermore, train passages on the testing line exhibit a smaller variation in operation speeds compared to those in the throat area.

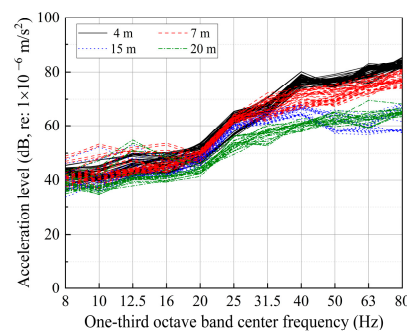


**Figure 16.** Measured vibration spectra of different train passages at various locations in the testing line area.

### 3.2.2. Architecture Determination of the DNN-RMDN Model

Similarly to Section 3.1.2, this section is dedicated to establishing the architecture of the DNN-RMDN model, which will serve as the foundation for Section 3.2.3, in which the model is adopted to quantify the uncertainty and predict the PDF of train-induced vibrations in the testing line area.

A total of 45 train passages were recorded at each of the four measurement locations, which were situated 4 m, 7 m, 15 m, and 20 m from the track center line. Consequently, a combined dataset comprising 1980 samples was obtained. Among them, 1386 randomly selected samples were allocated to the training dataset, with 594 samples designated for the testing dataset. The identical DNN model architecture outlined in Section 3.1.2 was employed in this context.

Figure 17a illustrates the mean squared error of the DNN model as the training epochs increase, showing convergence at 400 epochs. Figure 17b compares the predictions from the trained DNN model with the corresponding testing datasets. A linear regression with an  $R^2$  value of 0.965 indicates a strong correlation between them, suggesting that the trained DNN model performs effectively with the unseen testing datasets.

In Figure 18a, variations in calculated standard deviations at 31.5 Hz are depicted with different numbers of neurons in the hidden layer of the MLP and various numbers of Gaussian kernels within the mixture density model. Notably, the standard deviation of the dataset's residuals shows minimal sensitivity to the number of neurons in the 1-layer MLP, aligning with the detrending process where means predicted by the DNN model are subtracted from the training dataset. Figure 18b illustrates the variations in calculated standard deviations as the number of Gaussian kernels increases. It has been noted that the estimated standard deviations reached a stable value after incorporating more than 20 Gaussian kernels. This suggests that an order of the mixture density model

exceeding 20 is necessary to effectively capture the randomness in the dataset's residuals. Thus, the chosen architecture for the RMDN model comprises a one-layer MLP with 10 neurons and a mixture density model with 20 Gaussian kernels. Figure 18c displays the negative log-likelihood loss function of the RMDN model, converging at 6500 epochs for all 11 investigated center frequencies. The learning rate utilized is 0.0001. The error analysis, validation process, and uncertainty quantification utilizing the outcomes of the DNN-RMDN model are discussed in the subsequent section.

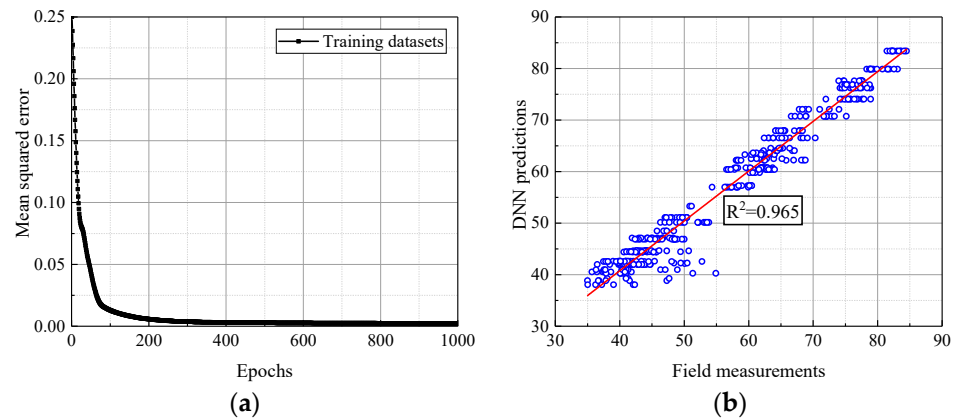


**Figure 17.** DNN model validation: (a) training process; (b) testing results.

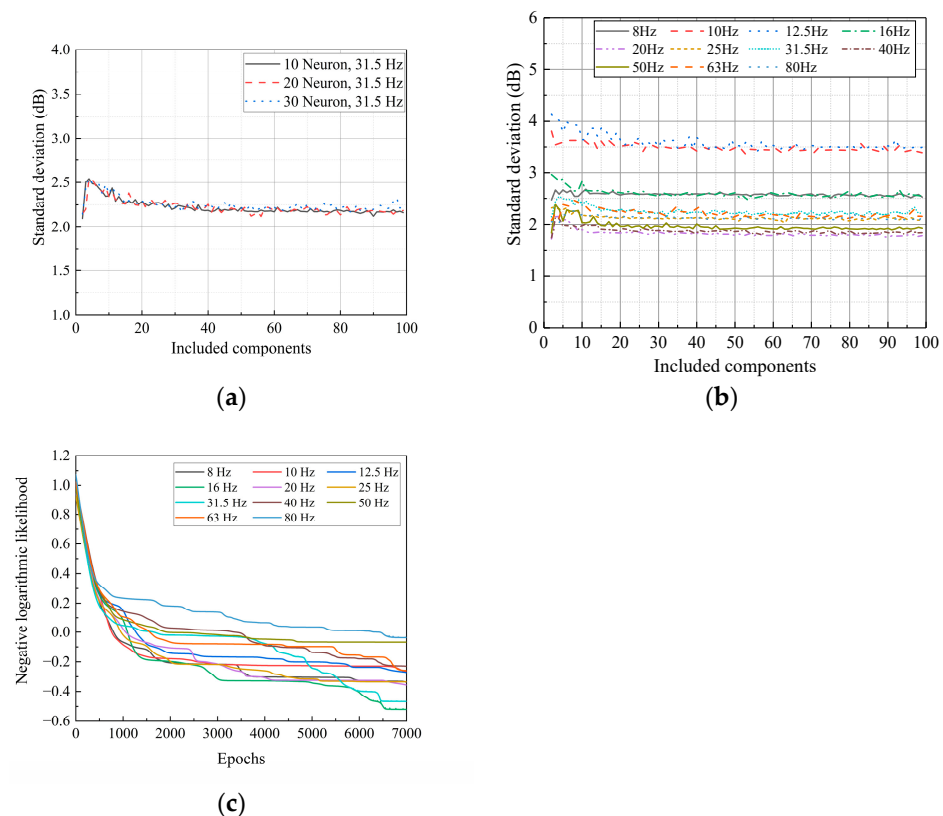


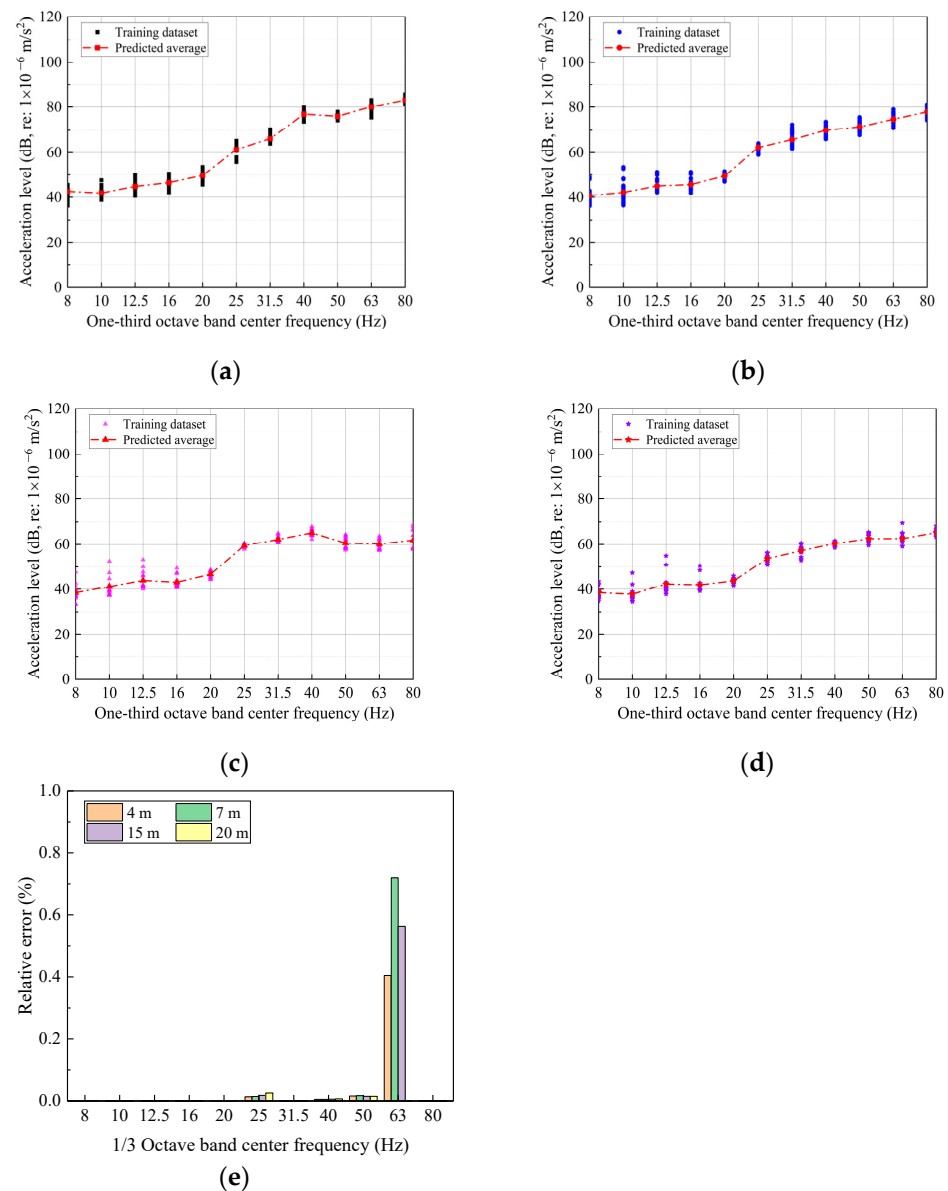
**Figure 18.** Sensitivity analysis for number of hidden neurons and Gaussian kernels: (a) effects of numbers of neurons and Gaussian kernels on  $\sigma$  at 31.5 Hz; (b) effects of numbers of Gaussian kernels on  $\sigma$  at different frequencies; (c) training process.

### 3.2.3. Quantifying Uncertainty with PDFs

This section presents the training and testing results of the DNN-RMDN model developed in Section 3.2.2. The predicted PDFs of train-induced vibration levels will be utilized as a foundation for conducting probabilistic assessments in Section 4.

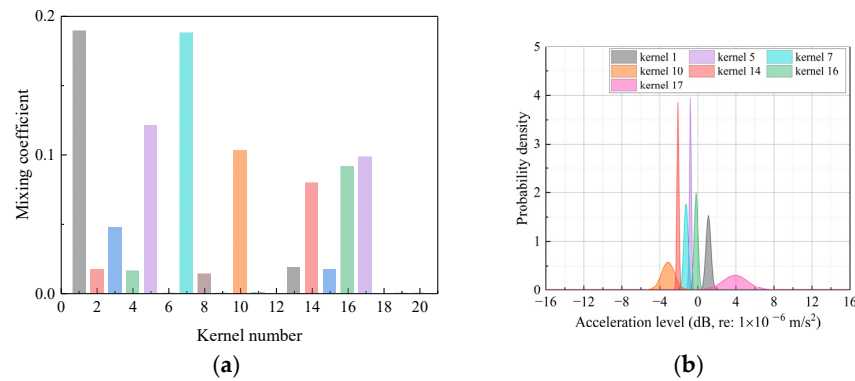


Figure 19 compares the predicted conditional averages of train-induced vibrations at the four measured locations using the trained DNN model to the training dataset. The percentage error is noted to be below 0.8%, as indicated in Figure 19e. It can be found that the DNN model is effectively trained and capable of capturing the conditional average train-induced acceleration levels at each center frequency and measurement location.



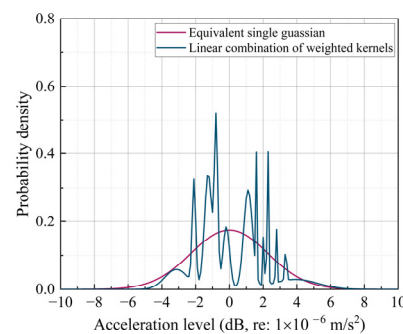
**Figure 19.** Predictions of conditional averaged vibrations using trained DNN model: (a) 4 m; (b) 7 m; (c) 15 m; (d) 20 m; (e) relative error.

Following the prediction of conditional average vibrations, the residuals of the dataset are used by the RMDN model to estimate their PDFs as a function of frequency. Figure 20a illustrates the mixing coefficients of the 20 Gaussian kernels in the mixture density model after training the DNN-RMDN model. Figure 20b displays the PDFs of the Gaussian kernels with significant mixing coefficients, which capture the patterns and characteristics of the residual dataset that have a higher likelihood of occurring. By comparing Figure 20a with Figure 11a, it is seen that the distribution of mixing coefficients for ground vibration at 31.5 Hz induced by train passages in the throat area is more uniform than that for ground vibration at the same frequency induced by train passages on the testing line. This indicates that PDF fitting with greater variability requires more kernel components.



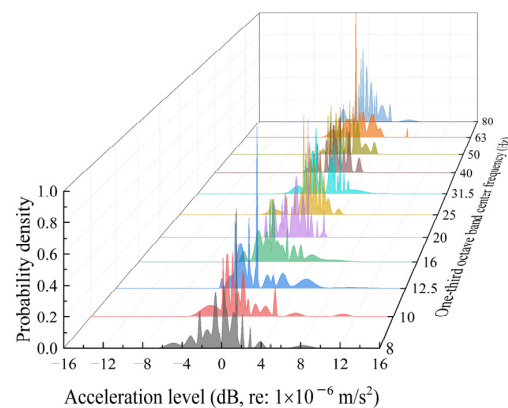
**Figure 20.** Mixing coefficients and Gaussian kernels PDF with larger coefficient (31.5 Hz): (a) mixing coefficients; (b) kernels with large mixing coefficient.

Figure 21 compares the overall PDF of residual train-induced vibrations at 31.5 Hz, based on the mixture density model consisting of a linear combination of 20 weighted Gaussian kernels shown in Figure 20, to the equivalent single Gaussian distribution with a mean of zero and standard deviation calculated from the residual dataset using Equation (3). Similarly to Figure 12, it is evident that the mixture density model has the capability to capture complex PDFs compared to a single Gaussian assumption. In addition, the residual PDF of train-induced acceleration levels in the testing line area exhibits a narrower range compared to that in the throat area.



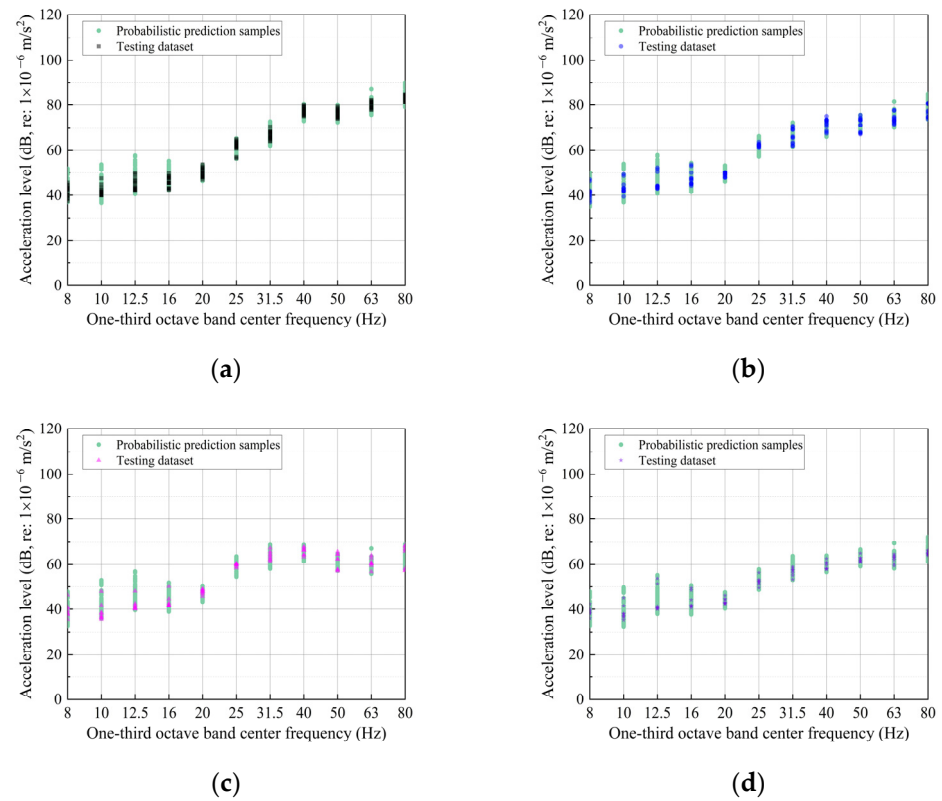
**Figure 21.** Comparisons of the PDF predicted with RMDN model and the Gaussian distribution.

Figure 22 presents the predicted PDFs of residual train-induced vibrations by the RMDN model at various center frequencies within the one-third octave band. The predicted PDFs of the RMDN model exhibit variations across different frequencies, indicating that the probability of exceeding the limit required by the standard also differs at each frequency. Identifying the frequencies with higher probabilities of exceeding the limit will assist in the design of vibration control measures.



**Figure 22.** PDFs predicted with RMDN model at different center frequencies.

The PDFs of train-induced vibration levels at each measurement location and frequency are obtained by combining the conditional averages predicted by the DNN model, as shown in Figure 19, with the PDFs of the residual dataset predicted by the RMDN model, as shown in Figure 22. Using the overall PDFs, 100 samples of acceleration level spectra are generated for each distance from the track centerline of the testing line. Figure 23 overlays these samples from the predicted PDF with the unseen testing dataset acquired from field measurements. It is evident that the testing dataset aligns well within the range of samples from the predicted PDF at different distances away from the track, thus validating the performance of the proposed DNN-RMDN method in probabilistic predictions.



**Figure 23.** Performance test of the trained DNN-RMDN model: (a) 4 m; (b) 7 m; (c) 15 m; (d) 20 m.

#### 4. Probabilistic Assessment of Train-Induced Vibrations

Building upon the probabilistic prediction and uncertainty quantification presented in Section 3.1 for train-induced vibrations in the throat area and Section 3.2 for the testing line area, this section introduces a probabilistic assessment method. In this section, the assessment standard outlined in the FTA guideline [7] is employed, with a selected limit of 72 dB for train-induced ground-borne vibrations in terms of velocity level. The limit is mandatory for each center frequency within the one-third octave band up to 80 Hz.

The predicted PDF  $p(V|d, f)$  of train-induced velocity levels using the DNN-RMDN model is expressed by Equation (6). It comprises the conditional average,  $\bar{V}_{avg}(d, f)$ , which is a function of distance to the track and frequency, predicted by the DNN model, and the residual PDF  $p(\Delta V|f)$ , which is a function of frequency predicted by the cascaded RMDN model:

$$p(V|d, f) = \bar{V}_{avg}(d, f) + p(\Delta V|f) \quad (6)$$

The probability of train-induced velocity levels exceeding the limit at a specific distance from the track and a fixed frequency can be calculated as follows:

$$P(V > V_{lim}|d, f) = 1 - \int_{-\infty}^{V_{lim}} p(V|d, f) \quad (7)$$

The black solid lines in Figure 24 illustrate the PDFs of train-induced vibrations in the throat area at 4 m from the nearest track centerline and frequencies of 31.5 Hz and 50 Hz, respectively. The red dashed lines correspond to the velocity level limit of 72 dB. The shaded areas beneath the PDFs represent the probability of exceeding the limit for each frequency at the specific location. It is evident that, for the given configuration, the probability of exceeding the limit at 50 Hz is greater than that at 31.5 Hz.

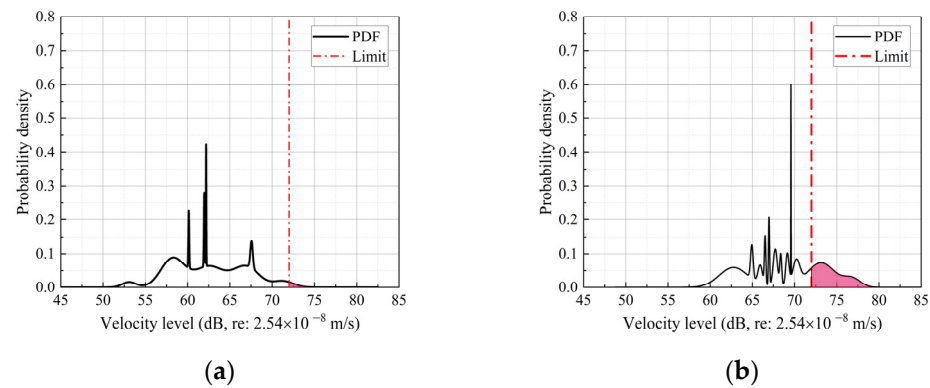


**Figure 24.** Usage of predicted PDF for calculating exceeding probability: (a) 4 m, 31.5 Hz; (b) 4 m, 50 Hz.

Figure 25 presents the contour of the probabilistic assessment of train-induced ground-borne vibrations in the throat area at various distances from the tracks and frequencies. It is intuitive to find that train-induced vibrations in the throat area, ranging from 50 to 63 Hz and occurring within 5 m from the nearest track centerline, have a 29% probability of exceeding the limit. The lower probability of exceeding vibration limits can be attributed to the implementation of ballast mattresses on the studied rail lines within the metro depot. These ballast mattresses effectively control and mitigate train-induced vibrations.

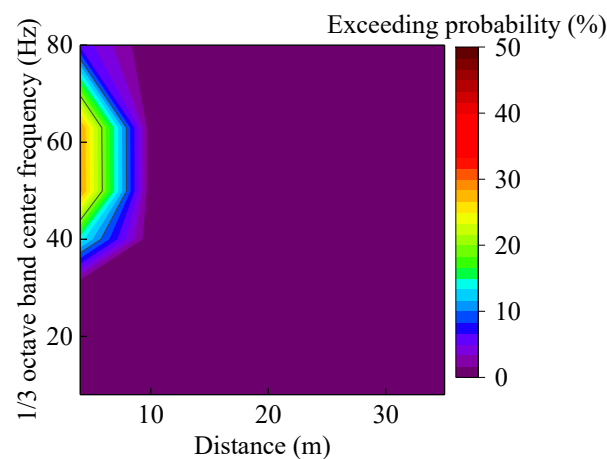


**Figure 25.** Probabilistic assessment of train-induced ground vibrations in the throat area.

The probabilistic assessment of train-induced vibrations across a wide field range and broad frequency range can be achieved very efficiently in a few seconds based on the predicted PDFs. Thus, the proposed DNN-RMDN method provides a valuable tool in practical applications for planning over-track buildings in complex vibration environments and making informed decisions regarding the design of vibration control measures.

The proposed model is trained and tested using the Python (3.12) language, making it easily integrable with various commercial FEM software like ABAQUS 2017. In practical implementation, only the distance to the track centerline and the investigated center frequency are necessary as data inputs. The model's outputs, which encompass the train-induced ground-borne vibrations and their distributions, can be imported into existing building vibration prediction software as external excitations. Moreover, through the

model's implementation, it becomes feasible to predict the probability of ground vibration surpassing the standard at specified distances and frequencies. This capability can assist in selecting building locations with varying vibration requirements and in determining the level and effective frequency range for vibration isolation measures. This approach helps avoid the indiscriminate use of excessively high-level isolation measures or the incorrect selection of the effective frequency range for isolation measures.

## 5. Conclusions

Field measurements have revealed significant variations in train-induced ground-borne vibrations within a metro depot, even when operating the same type of metro trains at similar low speeds. This research introduces a probabilistic prediction and assessment method, referred to as the DNN-RMDN model, which combines deep learning techniques with a mixture density model. The paper demonstrates the predictive accuracy of the proposed model using a theoretical benchmark example. Subsequently, the DNN-RMDN model is applied to a case study involving two extensive measurement campaigns, aiming to investigate and quantify the random nature of train-induced vibrations in both the throat area and the testing line area of the metro depot. The performance of the DNN-RMDN model remains robust when applied to practical train-induced vibration datasets that exhibit large or medium variations. It demonstrates reliable probabilistic prediction capabilities in such scenarios.

The application of the DNN-RMDN model involves the utilization of a deep neural network (DNN) model to predict the conditional average of train-induced vibrations. Subsequently, a mixture density model with a one-layer shallow multiple layer perceptron is employed to extract the probability density function. The throat area, characterized by a more complex track configuration, variations in measured trains, and varying distances between vibration sources and measurement points, exhibits higher uncertainty in ground vibrations caused by train operations compared to the testing line section. The distribution of weights of the Gaussian kernels in the RMDN model is more evenly distributed in the throat area. By employing a mixture density model instead of a single Gaussian distribution, the DNN-RMDN model achieves a more accurate prediction of the PDF for train-induced vibrations. The predicted PDFs enable efficient probabilistic assessment of train-induced vibrations across a wide field range and broad frequency range, with results obtainable in a matter of seconds. In conclusion, the proposed DNN-RMDN model serves as a practical tool for planning over-track buildings in complex vibration environments and making well-informed decisions regarding the design of vibration control measures.

Due to constraints in the available data, only the distance between the track and observation points along with the center frequency of the 1/3 octave band were considered as inputs in this study. While these limitations in the datasets can help manage uncertainty sources and provide data with increased fidelity and stronger correlations between the data and the analyzed input factors, incorporating other significant uncertainty sources like various rail types and operational conditions as inputs would enhance the model's versatility and scalability.

Given the challenge of controlling uncertainty sources across diverse field measurement datasets, it becomes essential to utilize numerical simulations or surrogate models. To enhance the model's robustness and applicability, future efforts may involve acquiring more extensive datasets covering a range of rail types and operational settings, developing numerical or surrogate models to address the impacts of different uncertainty sources, and strengthening the DNN-RMDN model's adaptability through techniques like data fusion and transfer learning.

**Author Contributions:** Conceptualization, methodology, writing—original draft preparation, Z.T.; formal analysis, investigation, writing—review and editing, L.H.; software, validation, writing—review and editing, D.T.; resources, data curation, funding acquisition, C.Z. All authors have read and agreed to the published version of the manuscript.



**Funding:** This research was funded by the open funding project of the State Key Laboratory of Performance Monitoring and Protecting of Rail Transit Infrastructure (Grant No. HJGZ2022110).

**Data Availability Statement:** The original contributions presented in the study are included in the article, further inquiries can be directed to the corresponding author.

**Conflicts of Interest:** Author Lingshan He was employed by the Guangzhou Urban Planning and Design Survey Research Institute Co., Ltd. The remaining authors declare that the research was conducted in the absence of any commercial or financial relationships that could be construed as a potential conflict of interest.

## References

1. Kouroussis, G.; Verlinden, O. Prediction of railway induced ground vibration through multibody and finite element modelling. *Mech. Sci.* **2013**, *4*, 167–183. [\[CrossRef\]](#)
2. Hu, J.; Zou, C.; Liu, Q.; Li, X.; Tao, Z. Floor vibration predictions based on train-track-building coupling model. *J. Build. Eng.* **2024**, *89*, 109340. [\[CrossRef\]](#)
3. Costa, P.A.; Calçada, R.; Cardoso, A.S. Track-ground vibrations induced by railway traffic: In-situ measurements and validation of a 2.5 D FEM-BEM model. *Soil Dyn. Earthq. Eng.* **2012**, *32*, 111–128. [\[CrossRef\]](#)
4. Zou, C.; Li, X.; He, C.; Zhou, S. An efficient method for estimating building dynamic response due to train operations in tunnel considering transmission path from source to receiver. *Comput. Struct.* **2024**, *305*, 107555. [\[CrossRef\]](#)
5. Tao, Z.Y.; Zou, C.; Yang, G.R.; Wang, Y.M. A semi-analytical method for predicting train-induced vibrations considering train-track-soil and soil-pile-building dynamic interactions. *Soil Dyn. Earthq. Eng.* **2023**, *167*, 107822. [\[CrossRef\]](#)
6. *JGJ/T 170-2009*; Standard for Limit and Measuring Method of Building Vibration and Secondary Noise Caused by Urban Rail Transit. Ministry of Housing and Urban-Rural Development of the People's Republic of China: Beijing, China, 2009.
7. Federal Transit Administration. *Transit Noise and Vibration Impact Assessment Manual*; US Department of Transportation: Washington, DC, USA, 2018.
8. He, C.; Jia, Y.; Zhou, S. Semi-analytical method for calculating ground vibrations from a tunnel in a homogeneous half-space with an irregular surface. *J. Sound Vib.* **2024**, *591*, 118615. [\[CrossRef\]](#)
9. Qiu, Y.; Zou, C.; Hu, J.; Chen, J. Prediction and mitigation of building vibrations caused by train operations on concrete floors. *Appl. Acoust.* **2024**, *219*, 109941. [\[CrossRef\]](#)
10. Lombaert, G.; Galvín, P.; François, S.; Degrande, G. Quantification of uncertainty in the prediction of railway induced ground vibration due to the use of statistical track unevenness data. *J. Sound Vib.* **2014**, *333*, 4232–4253. [\[CrossRef\]](#)
11. Ma, M.; Li, M.; Qu, X.; Zhang, H. Effect of passing metro trains on uncertainty of vibration source intensity: Monitoring tests. *Measurement* **2022**, *193*, 110992. [\[CrossRef\]](#)
12. Sun, H.; Fang, Y.; Yuan, Z.; Weng, Z.; Ni, D. Analytical modeling for the calculation of underground train-induced vibrations in inhomogeneous soils with uncertainty. *AIP Adv.* **2021**, *11*, 115321. [\[CrossRef\]](#)
13. Auersch, L. Train-induced ground vibration due to the irregularities of the soil. *Soil Dyn. Earthq. Eng.* **2021**, *140*, 106438. [\[CrossRef\]](#)
14. Jones, S.; Kuo, K.; Hussein, M.; Hunt, H. Prediction uncertainties and inaccuracies resulting from common assumptions in modelling vibration from underground railways. *Proc. Inst. Mech. Eng. Part F J. Rail Rapid Transit* **2012**, *226*, 501–512. [\[CrossRef\]](#)
15. Jafari, A.; Ma, L.; Shahmansouri, A.A.; Dugnani, R. Quantitative fractography for brittle fracture via multilayer perceptron neural network. *Eng. Fract. Mech.* **2023**, *291*, 109545. [\[CrossRef\]](#)
16. Connolly, D.P.; Kouroussis, G.; Giannopoulos, A.; Verlinden, O.; Woodward, P.K.; Forde, M.C. Assessment of railway vibrations using an efficient scoping model. *Soil Dyn. Earthq. Eng.* **2014**, *58*, 37–47. [\[CrossRef\]](#)
17. Connolly, D.P.; Kouroussis, G.; Woodward, P.K.; Giannopoulos, A.; Verlinden, O.; Forde, M.C. Scoping prediction of re-radiated ground-borne noise and vibration near high speed rail lines with variable soils. *Soil Dyn. Earthq. Eng.* **2014**, *66*, 78–88. [\[CrossRef\]](#)
18. Paneiro, G.; Durão, F.O.; Costa e Silva, M.; Falcão Neves, P. Artificial neural network model for ground vibration amplitudes prediction due to light railway traffic in urban areas. *Neural Comput. Appl.* **2018**, *29*, 1045–1057. [\[CrossRef\]](#)
19. Fang, L.; Yao, J.; Xia, H. Prediction on soil-ground vibration induced by high-speed moving train based on artificial neural network model. *Adv. Mech. Eng.* **2019**, *11*, 1687814019847290. [\[CrossRef\]](#)
20. Tao, Z.; Hu, Z.; Wu, G.; Huang, C.; Zou, C.; Ying, Z. Train-induced vibration predictions based on data-driven cascaded state-space model. *Building* **2022**, *12*, 114. [\[CrossRef\]](#)
21. Liang, R.; Liu, W.; Li, C.; Li, W.; Wu, Z. A novel efficient probabilistic prediction approach for train-induced ground vibrations based on transfer learning. *J. Vib. Control.* **2023**, *30*, 576–587. [\[CrossRef\]](#)
22. Liang, R.; Liu, W.; Ma, M.; Liu, W. An efficient model for predicting the train-induced ground-borne vibration and uncertainty quantification based on Bayesian neural network. *J. Sound Vib.* **2021**, *495*, 115908. [\[CrossRef\]](#)
23. Liu, W.; Liang, R.; Zhang, H.; Wu, Z.; Jiang, B. Deep learning based identification and uncertainty analysis of metro train induced ground-borne vibration. *Mech. Syst. Signal Process.* **2023**, *189*, 110062. [\[CrossRef\]](#)
24. McLachlan, G.J.; Basford, K.E. *Mixture Models: Inference and Applications to Clustering*; M. Dekker: New York, NY, USA, 1988; Volume 38.

25. Bishop, C.M. *Mixture Density Networks*; Aston University: Birmingham, UK, 1994.
26. Guillaumes, A.B. *Mixture Density Networks for Distribution and Uncertainty Estimation*. Ph.D. Thesis, Universitat Politècnica de Catalunya, Barcelona, Spain, 2017.

**Disclaimer/Publisher’s Note:** The statements, opinions and data contained in all publications are solely those of the individual author(s) and contributor(s) and not of MDPI and/or the editor(s). MDPI and/or the editor(s) disclaim responsibility for any injury to people or property resulting from any ideas, methods, instructions or products referred to in the content.